

# PREDICTION OF SEPARATION INDUCED BUFFET OVER NOVEL WING CONFIGURATIONS

Michael I. Woods, University of Bath, UK  
Norman J. Wood, University of Manchester, UK

**Keywords:** *subsonic, high angle of attack, buffet, vortex, separation*

## Abstract

*The compromise between aerodynamics and stealth technology has resulted in the generation of wing planforms which are both novel in relation to existing aircraft and unfamiliar to aerodynamicists concerned with the prediction of steady and unsteady aerodynamic loads. It is necessary to be able to predict these loads such that they can be minimised during the early design stage of an aircraft, and then adequately accounted for from both strength and fatigue viewpoints during the detailed design process.*

*This paper presents the buffet experienced by a lambda wing model, and details an initial step toward a prediction methodology for use as a design tool. The RMS buffet and the spectral content of the pressure fluctuations can be estimated from a mean pressure distribution, whether derived experimentally or using computational techniques.*

## Nomenclature

a	addition parameter
$\bar{c}$	mean aerodynamic chord
$C_p$	pressure coefficient
f	frequency
k	dissipation parameter
$\bar{n}_m$	modified reduced frequency
$\bar{p}$	RMS pressure
q	dynamic pressure
s	wing semispan
U	freestream velocity
w	thickness of shear layer
x	chordwise distance from apex
y	spanwise location

## 1 Introduction

Both manned and computerised simulation of air combat [1] have shown that in short range combat encounters aircraft tend to engage in a sequence of head-on passes. After each pass, during which weapons are released, both aircraft attempt to reverse course as quickly as possible to obtain another firing opportunity. In the course of such manoeuvring aircraft often exceed their maximum sustainable turn rate, reducing speed dramatically. Maximum instantaneous turn rates are thus limited by structural limits at moderate and high Mach numbers and by the maximum attainable lift at low speeds. The ability to aim the fuselage independently of flight path allows aircraft to utilise gunfire as an effective weapon, with rapid pitching manoeuvres bringing the weapon to bear as the combating aircraft pass. Maximum usable lift, together with a high thrust to weight ratio to replace the energy deficits resulting from the use of extreme manoeuvres are therefore of paramount importance when designing for modern short range combat.

Obviously, if an opponent can be engaged without counter-detection the initial manoeuvring becomes much simplified; the pilot simply manoeuvres to achieve a firing position and releases the weapon. The technology to achieve such a situation is generally concentrated on the reduction of the radar cross-section (RCS) of the aircraft and, equally importantly, the reduction of radar and infra-red emissions from the aeroplane. The former of these approaches is often apparent from the external shape of a modern aircraft.

However, for a future air-superiority or strike aircraft, stealth properties alone will not be sufficient. Stealth is much less important in short range combat when compared to the significant advantage that it can imbue at medium and long range. The aircraft must therefore be able to achieve the extreme manoeuvres required for successful short range encounters described earlier.

When a stealthy aircraft manoeuvres to the high angles of attack required for short range combat it is possible that large amounts of flow induced excitation (buffet) would be encountered. Should the frequency distribution of the buffet overlap with one or more structural modes then significant response of the structure (buffeting) may result. This is clearly undesirable and may result in a reduction of the flight envelope and/or in-service repair or replacement modifications. Such problems have been encountered in the past, particularly with reference to the fins of combat aircraft. A specific problem was encountered with the twin-fin F-18, where accelerations experienced at the fin tip were of the order of 500g [2]. This problem was solved by a dual approach. Strakes were added to alter the vortex track and the stiffness of the fin structure was increased to separate the frequency of the excitation and the natural frequency of the fin. Both of these approaches are unsatisfactory if a similar problem is encountered on a low-observable aircraft toward the end of the design process. The addition of strakes to a stealthy aircraft has a prohibitive RCS penalty and the complexity of the internal structure described earlier makes increases in structural strength costly from a weight, and hence performance, perspective.

It is therefore desirable to predict buffet loads during the early design stages of an aircraft such that they can be accounted for from both strength and fatigue viewpoints during the detailed design process. However, initial prediction of buffet loads currently relies on experience of the levels of buffet over aircraft already in service. For example, buffet information for EF-2000 was estimated after

consideration of the buffet loads experienced by the Tornado. There is currently no experience of the buffet encountered by a low-observable aircraft and it was felt that a more scientific method of estimating the buffet loads over such an aircraft was required. Such a method was likely to take advantage of the ability of contemporary steady state Computational Fluid Dynamics (CFD) codes to accurately predict vortex strength and track.

## 2 Experimental Details

To facilitate the acquisition of sufficient data to allow a prediction methodology to be realised at a reasonable cost, a new technique to acquire unsteady aerodynamic data was developed. This utilised a simple Scanivalve unit, more generally used for measuring mean/steady pressures. The tubing connecting the tappings to the Scanivalve unit were dynamically calibrated such that the pressure fluctuations at the tapping could be deduced from those measured at the Scanivalve unit. This technique has been demonstrated [3] to be able to accurately measure wing buffet at frequencies of up to 500Hz.

The wind tunnel models were constructed using a composite/foam technique to allow stiff, lightweight models to be manufactured in short timescales with minimal machining costs. The models were semi-span mounted in the 2.12m x 1.51m wind tunnel at the University of Bath. At typical test conditions the turbulence intensity was of the order of 0.5% and the Reynolds number in the working section was  $2.0 \times 10^6 / \text{m}$ .

## 3 Experimental Results

The main characteristics of the buffet experienced over the models tested will be described in this Section. These features must be identified by a prediction methodology, for it to have any value. Results are presented for a “lambda” planform, although similar trends were found for other models with the same sweep angles.

### 3.1 RMS Buffet

A plot of the typical RMS buffet over the lambda model is depicted in Figure 1. There is a region of high RMS pressure, which extends from the apex to the reverse apex. The magnitude of the pressure fluctuations varied slightly throughout this region. The variation in the magnitude and location of the high RMS region as the angle of attack of the model was increased is depicted in Figure 2. The region was found to be located inboard of the core of the leading edge vortex, in its attachment region.

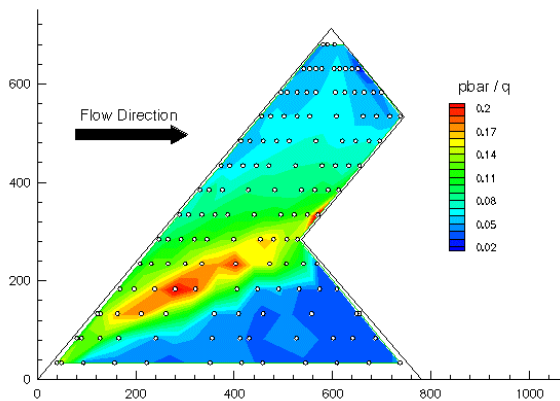


Figure 1: RMS pressures,  $\alpha = 14^\circ$

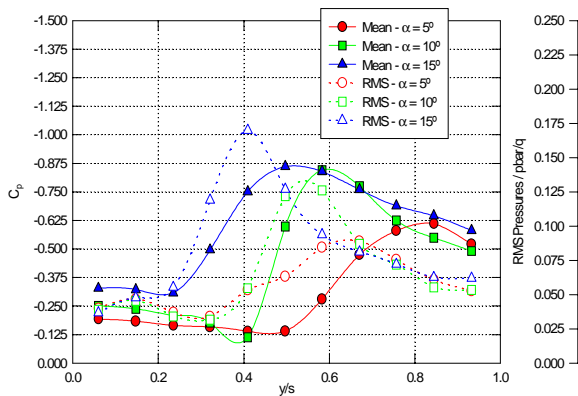


Figure 2: Relative location of suction peaks and RMS pressures

A possible explanation of the spanwise location of the peak in the RMS pressure fluctuations is depicted in Figure 3. Moving outboard from the centreline of the models, the RMS pressure fluctuations began to rise at the same spanwise location that the magnitude of the pressure coefficient began to rise. This location is the primary attachment line, which coincides with the outer limit of the shear layer.

The RMS pressures then rise as the core is approached, reaching a maximum just before the pressure coefficient rises to its maximum magnitude. It therefore seems likely that pressure fluctuations present within the shear layer are convected along with the layer. As the layer impacts the surface the pressure fluctuations are swept outboard, toward the vortex core. Fluctuations are added at a location slightly further outboard, and the sum of these oscillations is again swept outboard. This continues until the inside of the shear layer is reached and no further pressure fluctuations are added. As the fluctuations are swept outboard they will also dissipate due to viscous effects. Thus, the spanwise variation of the amplitude of the RMS pressures will depend on the relative strengths of two effects: the rate of increase of the fluctuations due to addition from the shear layer and the rate of dissipation.

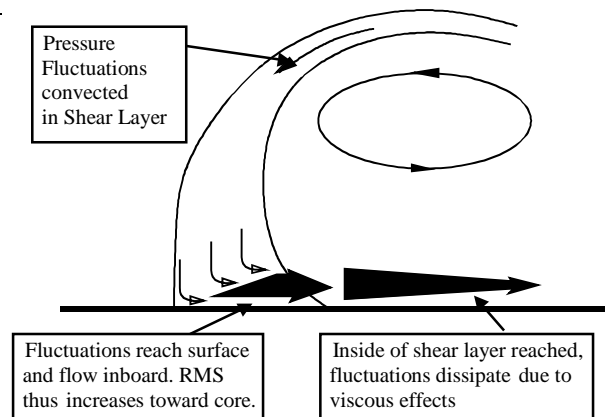


Figure 3: Increase of RMS pressure across shear layer

### 3.2 Buffet Spectra

As is clear from Figure 4, there is a distinct variation in the character of the spectra with spanwise location. At the point inboard of the primary attachment, where the RMS buffet is very small, there is little excitation throughout the frequency range examined (not depicted).

When the power spectra in the primary attachment region are examined (a), where the RMS buffet has risen, a broadband peak centred at a frequency of approximately 110Hz can be discerned. As the region where RMS buffet is at

a maximum is approached (b), there is a distinct change in the power spectra. Now, rather than just the single peak that was present further inboard, there are two peaks in the spectra. The first peak is centred at a frequency of approximately 75Hz whilst the second is centred at a frequency of 150Hz. Within the resolution that can be determined ‘by eye’ the frequency of the second peak is double that of the first; they are harmonics. Furthermore, when the broadband peak is considered it can be seen that it occurs at a frequency midway between the two harmonic peaks.

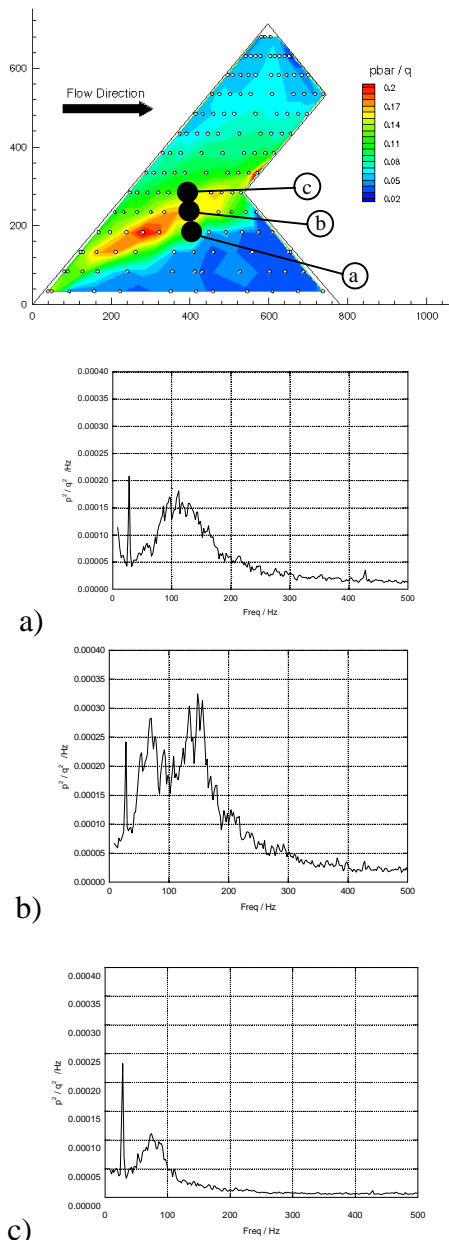


Figure 4: Spanwise variation of power spectra

If the buffet spectrum outboard of the ‘double peak’ location is examined (c), it can be seen that a single peak is present, as measured by other researchers [4,5]. However, the magnitude of the peak is much reduced from that experienced further inboard. Moving further outboard again, there is a single peak at the lower of the frequencies. The magnitude of the peak has decayed further (not depicted).

The demonstration of the presence of three distinct frequencies is a very important result. If predictions of buffet had been based on previous experimental data they would have predicted incorrect centre frequencies, since neither the higher frequency of the ‘double peak’ spectra or the intermediate frequency in the attachment region would have been predicted. The lower of the frequencies in the ‘double peak’ spectra is consistent with those found when examining single fin buffeting [6] over delta wings.

The variation in the centre frequencies over the model is summarised in Figure 5. Previous investigations of fin-buffeting at the University of Bath [6,7] had resulted in the use of a non-dimensional frequency parameter such that:

$$n_m = \frac{f c \sin \alpha}{U}$$

where  $f$  was the centre frequency of the peak buffet and  $c$  the aerodynamic mean chord. Since it seemed likely that the frequency was varying inversely with the distance from the apex,  $x$ , this frequency parameter was modified such that:

$$n_m = \frac{f x \sin \alpha}{U}$$

Lines representing constant values of  $n_m$  are also displayed on Figure 5. It can be clearly seen from this representation that the many of the centre frequencies follow lines of constant frequency parameter. In particular, a large number of tappings display peaks at frequencies corresponding to modified frequencies between 0.27 and 0.33. This corresponds to the lower of the ‘double peak’ frequencies as depicted in Figure 4. Another cluster of peaks is present at

modified reduced frequencies of between 0.57 and 0.60 where  $x < 420\text{mm}$ . These peaks correspond to the higher of the ‘double peak’ frequencies. It should be noted that these high frequency peaks are less common than those at the low frequency are. This indicates the limited number of locations at which the high frequency peaks are present.

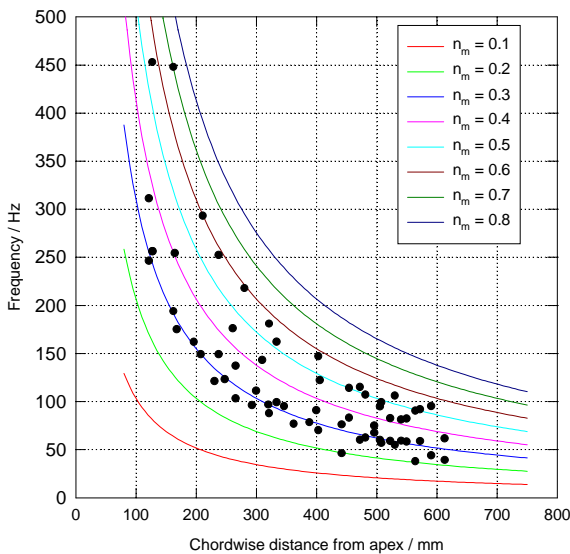


Figure 5: Variation of centre frequencies with chordwise location

## 4 Buffet Prediction Methodology

### 4.1 Overview

The aim of a wing buffet prediction tool is to be able to predict the power spectra acting over the entire surface of the wing. This would comprise a complete description of the spectra, including the frequencies at which peaks occur, the magnitude of the peaks and the shape of the peaks. The importance of this last criterion, the *shape* of the peaks in the buffet spectra, should not be underestimated since it will be of critical importance when the response of the structure due to buffet (buffeting) is calculated. A spectrum with a sharp peak at a frequency will cause little buffeting until a flight condition is reached that causes interaction between the buffet and the narrow resonance peak, due to low structural damping, of the structure. Conversely, a broad peak will cause a response

throughout the speed/incidence range of the aircraft.

A complete description of the buffet spectra would lead to a simple derivation of the RMS buffet acting over the wing, since the RMS buffet can be calculated by simply considering the area under the power spectra. Therefore, prediction of the buffet spectra presents the broadest prediction method necessary. However, this approach requires the following parameters to be calculated at all points over the wing:

- The frequency/frequencies at which buffet is a maximum
- The magnitude of the buffet at each of these frequencies
- A measure of the breadth of the peaks

It was with these criteria in mind that a curve-fitting program was written. This resulted in up to seven parameters to describe each power spectra, which was described as the superposition of base excited mass/spring/damper systems:

- The natural frequency/frequencies of each system
- A forcing amplitude for each system
- The damping of each system

In addition to these parameters, an additional constant amplitude function was added such that noise in the system could be accounted for. Comparison of the requirements and the output of the program indicate that the parameters output by the system were ideal for the development of a prediction methodology.

However, despite the large number of tappings built into each wing, there were still relatively few areas over the wing at which phenomena such as double peaks in the spectra were apparent. For example, over the lambda wing at an incidence of  $14^\circ$  there were eight tappings where double peaks were apparent and only three where the ‘intermediate frequency’

peak was apparent. Also, as was evident from the scatter plots of the centre frequencies, there was a large spread of centre frequencies with no obvious trend in the variation of the *spread* as the incidence or planform was changed. Therefore, it is difficult to speculate as to the cause of the variation. However, any buffet data acquired is susceptible to the natural statistical variation present in any such stochastic process, and it seems possible that this is the cause of much of the spread in the data.

Hence, since such variation in the RMS pressures was known, (it was tested at the start of each wind-tunnel test) it was decided to pursue an alternative route to predicting the buffet spectra. This would involve the prediction of the RMS pressures as the first step in the process. The next step would be to predict the number and frequencies of the peaks in the power spectra. The shape of the peaks would then be estimated and the relationship between the RMS pressures and the power spectra would then be utilised to derive the power spectra.

A first step toward this approach is demonstrated in this paper. The reconstruction of the RMS pressures and PSDs over the lambda wing is undertaken. This reconstruction could then be applied to the other models and, if successful, a step toward a prediction methodology would have been made. It should be noted that this is intended as a demonstration that such a concept is feasible, and that this approach has the potential to be extended such that separation induced pressure fluctuations can be predicted over aircraft at an early design stage. It is proposed as a first step to such a methodology, and significant development of this technique is required to enable its use in a design environment.

#### 4.2 Reconstruction of RMS Buffet

A schematic diagram of a typical spanwise RMS pressure distribution is depicted in Figure 6. A low level of excitation is found at the centreline of the model. The level of RMS buffet then stays approximately constant until

the outer edge of the shear layer is reached, where it begins to rise rapidly. The RMS level of pressure fluctuations reaches a peak slightly inboard of the core of the vortex before decaying outboard of the vortex core. It was proposed in Section 3.1 that, at points on the wing between the primary attachment line and the vortex core, there were two competing effects present. These effects were the rate of addition of fluctuations from the shear layer and the rate of dissipation of any unsteadiness present in the flow. Therefore, if the rates of addition and dissipation can be predicted together with the level of excitation at the centreline of the model, the level of RMS excitation over the planform can be calculated.

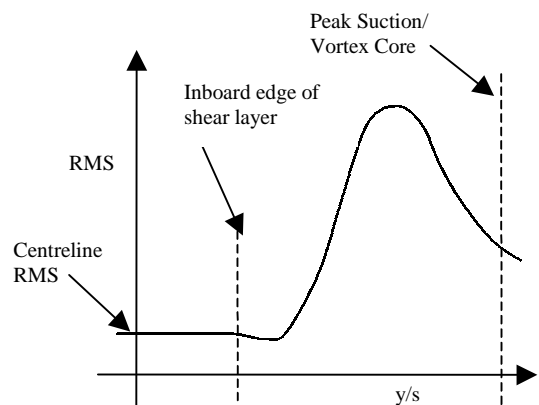


Figure 6: Schematic of Spanwise RMS Pressure Distribution

If this model of conflicting addition and dissipation is applied to the spanwise distribution of RMS pressures over the lambda wing model, where propagation is only noticeable downstream, a simple exponential fit can be made to represent the decay of the pressure fluctuation *outboard* of the shear layer where:

$$\frac{\bar{p}}{q} = \left( \frac{\bar{p}}{q} \right)_{\max} e^{-k \left( \frac{y - y}{s \quad s_{\max}} \right)}$$

This assumes that at points outboard of the vortex core there is no addition term, but that the dissipation process continues. Spanwise slices were taken through the steady and RMS pressure distributions over the lambda wing model. A simple Visual Basic program within

Microsoft Excel was then utilised to locate the points of maximum suction and perform a least squares fit to estimate the constant,  $k$ . The variation of  $k$ , the rate of dissipation, is plotted against incidence at a number of chordwise stations in Figure 7. Two observations can be made from this graph, upon which lines of best fit have been superposed. Firstly, at a given incidence the dissipation,  $k$ , which is based on non-dimensional spanwise location  $\frac{y}{s}$ , is larger toward the trailing edge of the model. Secondly, the dissipation changes more rapidly as the incidence is increased at the trailing edge of the model.

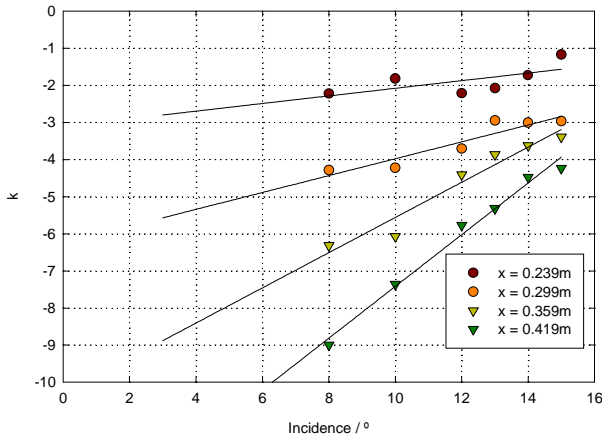


Figure 7: Variation in dissipation parameter with incidence and chordwise location

The gradients and intercepts of the lines of best fit are plotted in Figures 8 and 9. As is clear from these, a simple linear relationship between chordwise location, incidence and damping parameter can be derived such that:

$$k = (3.384x - 0.738)\alpha + (12.27 - 63.17x)$$

where  $x$  is the chordwise distance from the apex and  $\alpha$  is the incidence of the model measured in degrees. The damping parameter can therefore be calculated for an arbitrary chordwise location and incidence.

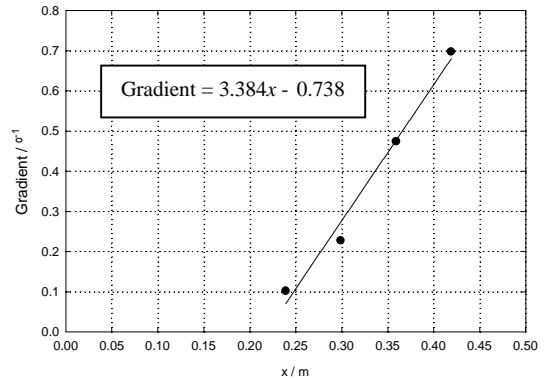


Figure 8: Variation of gradient of dissipation parameter with chordwise location

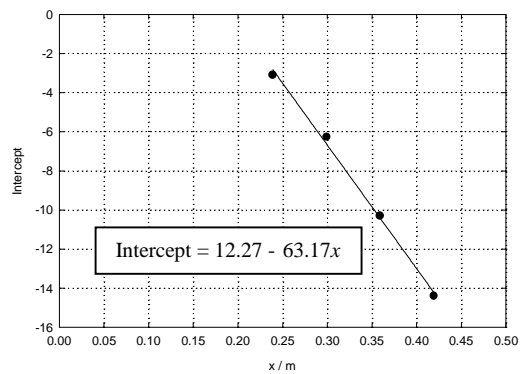


Figure 9: Variation of intercept of dissipation parameter with chordwise location

Once the damping parameter had been calculated by examining the decay of the pressure fluctuations outboard of the suction peak the other required parameter, the rate of additions from the shear layer, could be calculated. If the rate of the addition from the shear layer is assumed to be proportional to the pressure gradient, it follows that:

$$\frac{d(RMS)}{d\left(\frac{y}{s}\right)} = a \frac{dC_p}{d\left(\frac{y}{s}\right)} + k(RMS)$$

where  $a$  is the addition constant. This can be manipulated to give the expression:

$$RMS\left(\frac{y}{s}\right) = ae^{k\frac{y}{s}} \int e^{-k\frac{y}{s}} \frac{dC_p}{d\left(\frac{y}{s}\right)} d\left(\frac{y}{s}\right)$$

Hence, if the dissipation constant,  $k$ , is known together with the spanwise RMS distribution,  $RMS\left(\frac{y}{s}\right)$ , the addition constant  $a$  can be

calculated. The Microsoft Excel macro was enlarged to numerically calculate the integral. Use was also made use of Excel’s ability to iterate to calculate a least squares fit between the predicted and experimental values of RMS pressures, thus estimating a value for  $a$ .

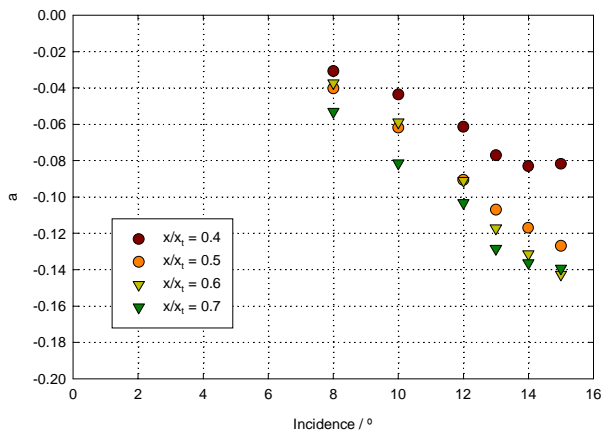


Figure 10: Variation of addition parameter with chordwise location and incidence

The calculated vales of  $a$  are plotted for a range of incidences and chordwise locations in Figure 10. The values of the addition parameter increase as the incidence increases, and grow toward the trailing edge of the model.

The circulation contained within a leading edge vortex increases approximately linearly with chordwise location [8], and it seems plausible to assume that the addition parameter might be related to the local circulation. Figure 11 depicts the addition parameter divided by chordwise distance from the apex, thus showing an approximate relationship between the addition parameter per unit of circulation, chordwise location and incidence. A linear relationship between addition parameter divided by chordwise location and incidence can now be determined, and this is superposed on Figure 11. Although there are deviations of approximately  $\pm 10\%$  between the experimental results and the linear relationship there does appear to be a strong correlation between this scaled parameter and incidence which is largely independent of the chordwise location of the points. Indeed, the largest deviations are found at the maximum incidence at which significant buffet was experienced. It has been indicated [8] that the

increase in circulation contained within the leading edge vortex as the incidence was increased was reduced as stall was approached. It can be hypothesised that the observed deviation from a linear relationship at higher incidences is due to this effect.

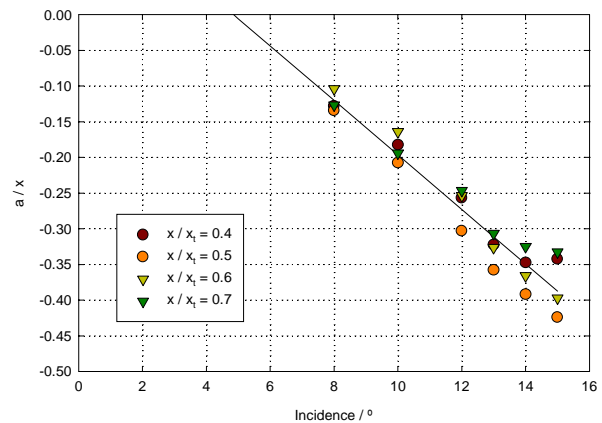


Figure 11: Variation of addition parameter divided by chordwise location

Nevertheless, this relationship between incidence, chordwise location and addition parameter can be utilised to estimate the addition parameter  $a$  using the relationship:

$$\frac{a}{x} = 0.1855 - 0.0382\alpha$$

where  $\alpha$  is measured in degrees.

The final parameter required to enable prediction of RMS buffet over the planform is the level of buffet at the centre of the model. This is plotted against the steady pressure coefficient at the centre of the model in Figure 12. There is a correlation between these two parameters which can be expressed as:

$$RMS = 0.0267C_p + 0.0539$$

All of the required parameters for reconstruction of the RMS pressures over the model can now be calculated at any point on the wing. There is a limitation to the scheme, however, in that it requires an uninterrupted spanwise slice to be available to calculate the RMS pressure distribution. It is therefore not possible to calculate the RMS pressure distribution at locations downstream of the reverse apex on the model.

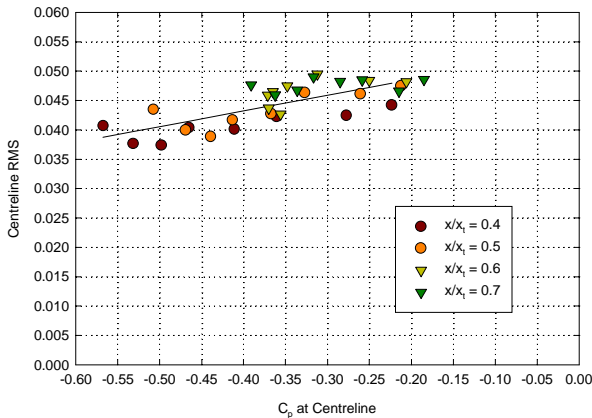


Figure 12: Variation of centreline RMS with centreline pressure coefficient

The relationships that have been derived during this analysis were utilised, together with another Visual Basic program, to calculate the RMS pressure distribution over the model at an incidence of  $14^\circ$ . The inputs to the program were spanwise steady pressure distributions at defined chordwise locations. The suction peaks were then identified, and the addition parameter  $a$ , the dissipation parameter  $k$  and the centreline level of RMS buffet were then calculated. These values then enabled the spanwise RMS pressure distributions to be calculated. A contour plot of the resulting RMS pressure distribution over the model at an incidence of  $14^\circ$  is depicted in Figure 13. This can be compared with the experimentally measured RMS buffet, which is displayed in Figure 14.

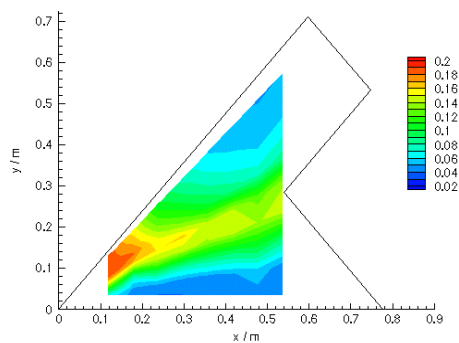


Figure 13: Calculated RMS pressure distribution

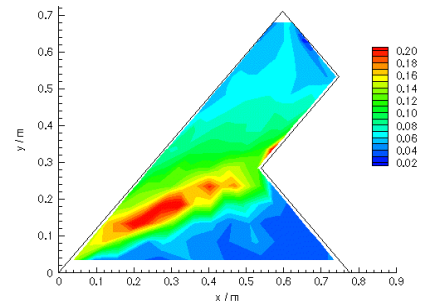


Figure 14: Experimental RMS pressure distribution

The spanwise locations of peak RMS buffet are well replicated by the calculations. This is largely controlled by the value of the ‘dissipation parameter’. However, the peak values of the RMS pressure are not as well represented, especially toward the rear of the calculated area. Maximum experimental values of RMS pressure were approximately 0.17 in this area, but predictions indicated that the maximum RMS pressure would be 0.15. This 11% error can be largely explained by the variation in the addition parameter indicated in the discussion of Figure 11.

The first necessity of a buffet prediction method, the reconstruction of levels of RMS buffet, has now been achieved. This will enable the magnitudes of the peaks of the PSDs to be estimated once the number, frequency and shape of the peaks has been estimated.

### 4.3 Forecast of Centre Frequencies

The concept of modified reduced frequency parameter,  $n_m$ , was introduced in Section 3.2, and it was shown that there were peaks corresponding to three distinct values of  $n_m$ . The lowest frequency of these peaks was present at the largest number of locations, and corresponded to modified reduced frequency parameter of 0.30. Deviations of  $\pm 10\%$  from this value of  $n_m$  were found over the wing.

The highest frequency peak was apparent at values of  $n_m$  between 0.57 and 0.60. These peaks were found in the regions of highest RMS and were rare, with only 8 tappings out of the 165 present over the wing experiencing two

peaks in their pressure spectra. Toward the trailing edge of the model the frequency of these peaks appeared to reduce, although this was possibly due to the difficulty of discriminating between two peaks with similar frequencies. This high frequency peak was always accompanied by the low frequency peak described in the previous paragraph.

The rarest of the peaks in the spectra were encountered in the region directly under the primary attachment line. The frequency of these peaks was approximately midway between the other two that were detected and corresponded to a reduced frequency parameter of 0.45.

It was decided to use the spanwise RMS pressure distribution to determine the number and frequency of the peaks that were present. Areas outboard of the high RMS region where two peaks were present experience only a single, low frequency, peak and areas inboard experience a peak of intermediate frequency. The frequencies of these peaks were defined by their modified reduced frequency parameter, as described previously.

#### 4.4 Estimation of Peak Shape

To enable the reconstruction of the power spectra, the shape of the peaks and the relative magnitudes of any peaks must be known in addition to their frequencies and RMS pressures. The damping of the peaks, as derived by the curve fitting program over the lambda wing at an incidence of  $14^\circ$  are depicted in Figure 15. The sizes of the symbols in this plot are proportional to the amplitude of the peaks that were detected. As is clear from this figure, there was no clear trend to enable the damping to be estimated accurately. Plotting the damping against modified reduced frequency parameter, as well as a number of other variables, was also undertaken. It was felt that a correlation between  $n_m$  and damping was most likely. This might have, for example, shown that the mid-frequency peak with  $n_m=0.45$  was a broader peak than the low frequency  $n_m=0.30$  peak. However, no correlation was found. It may be

that if more points in this ‘broadband peak’ area had been identified that such a correlation would be forthcoming.

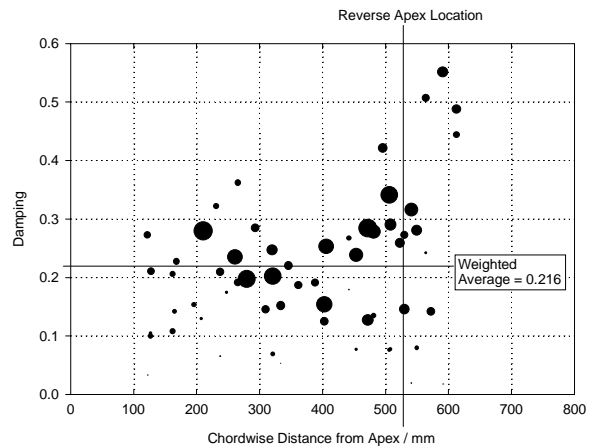


Figure 15: Damping of peaks

The only ‘relationship’ that was noted is depicted on Figure 15. It was found that the damping was somewhat affected by chordwise location. Plotting the damping against any other parameter or combination of parameters resulted in an even worse correlation, with points located entirely randomly over the plot. Although there is little in the way of a correlation between damping and chordwise location, it can be seen from Figure 15 that points upstream of the reverse apex generally correspond to dampings of between 0.10 and 0.30. Downstream of the reverse apex higher dampings are more commonplace.

To enable some estimate of the PSDs to be made, a weighted average of the damping of the peaks was made for locations upstream of the reverse apex. The weighting variable utilised was the amplitude of the peaks. This resulted in a weighted average damping of 0.216.

#### 4.5 Reconstruction of Power Spectra

The final remaining task to enable the reconstruction of the power spectra over the wing planform was to estimate the relative heights of the peaks at frequencies relating to reduced modified frequency parameters of 0.30, 0.45 and 0.58. As was stated in Section 4.3, it was decided to use the region of maximum

RMS pressure as a reference point to determine the frequency content of the PSDs.

This can be expanded upon to enable both the amplitude and frequency of the peaks to be estimated. This approach is depicted in Figure 16. The figure shows the relative amplitude of peaks at the three frequencies at a spanwise slice. The spanwise dimension,  $w$ , is the distance from the primary attachment line to the point of maximum RMS pressure. The distances indicated on the diagram have been derived by inspection of the PSDs over the surface of the models. The relative amplitudes of the  $n_m = 0.30$  and  $n_m = 0.58$  peaks result from the observation that PSDs have been measured where the amplitude of the high frequency peaks have been double that of the low frequency peaks. The scheme depicted allows for this event, although it will only be apparent in a very narrow region within the shear layer. The high frequency peak has not been noted outboard of the suction peak, so outboard of this location only the  $n_m = 0.30$  peak is present.

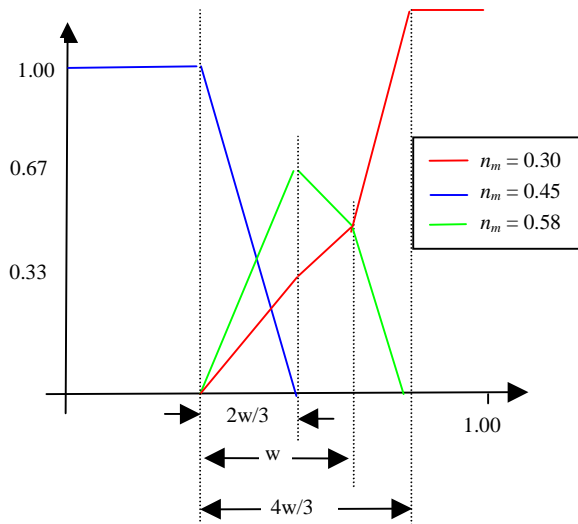


Figure 16: Relative amplitudes of frequency peaks

The full PSD reconstruction scheme can now be described:

- 1) Estimate the spanwise RMS distribution as detailed in Section 4.2.
- 2) Locate the spanwise location of the point of interest on Figure 16.

- 3) Subtract the centreline RMS from the calculated RMS. This is then placed as a white noise signal on the PSD.
- 4) The relative amplitudes of the frequency peaks, together with their damping ( $\zeta=0.216$ ) are now known. Iterate the amplitudes of these peaks to achieve the required RMS, calculated in Step 1).

Comparisons between estimated and measured PSDs over the surface of the Model are shown in Figure 17. The PSDs have been calculated using the above technique, including the estimation of the RMS pressures.

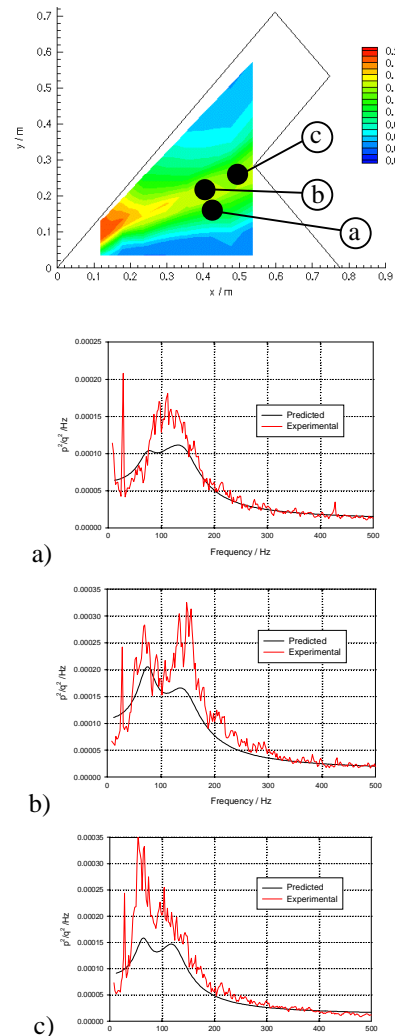


Figure 17: Comparison of predicted and experimental PSDs

The predicted frequencies match those measured experimentally extremely well. The magnitude of the peaks is not as well replicated.

This is largely due to errors in the RMS estimate at tappings. An error of 10% in the predicted RMS pressure results in a difference of 21% in the area under the PSDs, thus making the comparison look less satisfactory. To evaluate whether this is the cause of the differences between the predicted and actual PSDs, an advantage of the two-stage process could be utilised. The experimental values of RMS pressure could be utilised in Step 1) of the process, and the PSDs could then be calculated using Steps 2) to 4) using these values.

This observation indicates the importance of improved estimation of the addition parameter, possibly by examining any possible relationship between the circulation of the leading edge vortex and the parameter.

The shape of the predicted peaks is generally good, particularly for tapping b). This can be noted by examining the reduction in amplitude of the pressure fluctuations at higher frequencies, the predicted curve follows the experimental data closely.

## 5 Conclusions

A series of programs have been written to derive the variation of the rates of addition from the shear layer and dissipation at the surface of the model by considering the steady and RMS pressure distributions. These parameters have been plotted and can be reconstructed using simple relationships involving the chordwise location and model incidence. This has enabled the RMS pressure to be reconstructed if the steady pressure distribution is known.

Comparisons between the reconstructed and experimental RMS pressure distributions show good agreement in the spanwise location of maximum RMS pressure. However, the amplitude of the RMS pressure was less well reconstructed, with errors of up to 11% apparent.

The relationships between the chordwise location and frequencies at which excitation was

a maximum has enabled these frequencies to be estimated over the surface of the model. This, together with a very simple model of the distribution of the relative amplitudes of the three peaks in the spectra and estimates of the breadth of the peaks, has enabled the power spectra over the surface of the model to be predicted. The estimation of the centre frequencies of the peaks is very good, and the shape of the individual peaks is well replicated. However, the magnitude of the peaks is less well represented. This is largely due to the errors in the RMS pressure prediction, since an 11% error in RMS pressure fluctuations corresponds to a 21% error in the area under a PSD.

## 6 Acknowledgements

This research was funded by Engineering & Physical Sciences Research Council Grant number GR/J86902 in collaboration with British Aerospace (MA&A), RD1 ref.no. WAP04GAAN, R&D Activity 2.3.A.3.

## 7 References

- [1] Herbst W.B., Dynamics of air combat, *J. Aircraft*, Vol 20, No 7, pp. 594-598, 1983
- [2] Mabey D.G., Measurements of fin buffeting on an 'F-18' model and derived interpretive hypothesis, DRA Bedford, *Technical Memorandum Aero 2224*, 1991
- [3] Woods, M.I., Wood, N.J., Effect of sweep on buffet over novel wing planforms, *J.Aircraft*, in press
- [4] Gursul, I., Unsteady flow phenomena over delta wings at high angles of attack, *AIAA Journal*, Vol 32, No 2, pp.225-231, 1994
- [5] Hubner J.P., Komerath N.M., Spectral mapping of quasi-periodic structures in a vortex flow, *J. Aircraft*, Vol 32, No 3, pp. 493-500, 1995
- [6] Bean D.E., The analysis and suppression of vortex induced unsteady loads at high angles of attack, *PhD Thesis*, University of Bath, 1990
- [7] Chesneau T.R., Configuration dependent buffeting of a generic single fin combat aircraft, *PhD Thesis*, University of Bath, 1996
- [8] Nelson R.C., Visser K.D., Breaking Down the Delta Wing Vortex. The Role of Vorticity in the Breakdown Process, AGARD-CP-494, *Symposium of the Fluid Dynamics Panel*, Scheveningen, Netherlands, 1<sup>st</sup> to 4<sup>th</sup> October 1990